Neuro-Oncology 15(12):1615–1624, 2013.
doi:10.1093/neuonc/not129
Advance Access publication October 24, 2013

Multivoxel ^{1}H MR spectroscopy is superior to contrast-enhanced MRI for response assessment after anti-angiogenic treatment of orthotopic human glioma xenografts and provides handles for metabolic targeting

Bob Hamans, Anna Catharina Navis†, Alan Wright, Pieter Wesseling, Arend Heerschap, and William Leenders

Department of Radiology (B.H., A.W., A.H.) and Department of Pathology, Radboud University Nijmegen Medical Centre, Nijmegen, the Netherlands (A.C.N., P.W., W.L.); Department of Pathology, VU University Medical Centre, Amsterdam, the Netherlands (P.W.)

Present affiliation: Jeroen Bosch Hospital, Den Bosch, the Netherlands (B. H.)

Background. Anti-angiogenic treatment of glioblastoma characteristically results in therapy resistance and tumor progression via diffuse infiltration. Monitoring tumor progression in these patients is thwarted because therapy results in tumor invisibility in contrast-enhanced (CE) MRI. To address this problem, we examined whether tumor progression could be monitored by metabolic mapping using ^{1}H MR spectroscopic imaging (MRSI).

Methods. We treated groups of BALB/c nu/nu mice carrying different orthotopic diffuse-infiltrative glioblastoma xenografts with bevacizumab (anti–vascular endothelial growth factor [VEGF] antibody, $n = 13$), cabozantinib (combined VEGF receptor 2/c-Met tyrosine kinase inhibitor, $n = 11$), or placebo ($n = 15$) and compared CE-MRI with MRS-derived metabolic maps before, during, and after treatment. Metabolic maps and CE-MRIs were subsequently correlated to histology and immunohistochemistry.

Results. In vivo imaging of choline/N-acetyl aspartate ratios via multivoxel MRS is better able to evaluate response to therapy than CE-MRI. Lactate imaging revealed that diffuse infiltrative areas in glioblastoma xenografts did not present with excessive glycolysis. In contrast, glycolysis was observed in hypoxic areas in angiogenesis-dependent compact regions of glioma only, especially after anti-angiogenic treatment.

Conclusion. Our data present MRSI as a powerful and feasible approach that is superior to CE-MRI and may provide handles for optimizing treatment of glioma. Furthermore, we show that glycolysis is more prominent in hypoxic areas than in areas of diffuse infiltrative growth. The Warburg hypothesis of persisting glycolysis in tumors under normoxic conditions may thus not be valid for diffuse glioma.

Keywords: anti-angiogenic therapy, glioma, magnetic resonance spectroscopic imaging, tumor metabolism, Warburg effect.

Glioblastoma is a highly aggressive primary brain tumor with dismal prognosis. Current therapy consists of surgery to the maximum feasible extent, followed by local irradiation and chemotherapy with temozolomide. These treatments are, however, palliative rather than curative: almost without exception, glioblastomas eventually recur with fatal outcome, and median survival is currently still only 14.6 months.[1]

Glioblastomas characteristically contain areas of necrosis, surrounded by regions of active angiogenesis.[2] The lack of curative treatment options results from the presence of additional tumor zones in which cells infiltrate in a spiderlike pattern over considerable distances in the brain, often using white matter tracts or blood vessels as a scaffold and preventing radical surgery and radiotherapy. Diffuse infiltrative tumor growth does not strictly rely on neovascularization, as incorporated preexistent

Received March 1, 2013; accepted July 21, 2013.

†These authors contributed equally to this work.

Corresponding Author: William Leenders, PhD, Dept of Pathology, Radboud University Nijmegen Medical Centre, PO Box 9101, 6500 HB Nijmegen, the Netherlands (w.leenders@pathol.umcn.nl).

vasculature in these areas suffices to comply to the tumors' metabolic demands.[3] As the blood–brain barrier in these incorporated vessels is mostly intact, regions of diffuse tumor growth go largely unnoticed on contrast-enhanced (CE) MRI scans, which might result in an underestimation of tumor burden.[4–8] Also, the blood–brain barrier in diffuse infiltrative tumor areas complicates treatment with intravenously administered therapies.[9]

In the absence of curative treatment options, the presence of angiogenic areas in glioblastomas has made these tumors candidates for anti-angiogenic therapy.[10–12] Bevacizumab, a neutralizing antibody of vascular endothelial growth factor (VEGF) A, induces a radiological response in the majority of patients and may considerably improve quality of life.[5,13,14] Bevacizumab was FDA approved for treatment of recurrent glioma in 2009.

In the past years we have generated a number of orthotopic human glioma xenograft models by direct implantation of surgically obtained glioblastoma specimens in nude mice.[15] Unlike most cultured glioma cell lines that develop to circumscribed and angiogenic tumors upon intracerebral implantation (eg, U87[16]), our xenograft models have retained the capacity to grow via diffuse infiltration, sometimes concomitantly with local angiogenesis. It is increasingly recognized that these models that recapitulate the heterogeneous phenotypes of clinical glioma, including intact blood–brain barrier in diffuse areas, are of high value for preclinical investigations of antiglioma therapies.[17] We previously reported that treatment of diffuse glioma xenograft models with angiogenesis inhibitors (bevacizumab, vandetanib, sunitinib, and combinations thereof) affects compactly growing, angiogenesis-dependent regions in glioma but does not have an impact on the diffuse infiltrative phenotype.[4,7,9] These treatments did not improve overall survival in our models.

Whereas the perinecrotic angiogenic areas in clinical glioblastoma can be readily visualized in CE-MRI scans, this visibility drops rapidly when VEGF-targeted therapies are applied.[5,18] In our orthotopic glioma models, this effect is also observed, and it is well established that this does not represent an antitumor effect but is rather due to vascular normalization and (partial) restoration of the blood–brain barrier,[4,7,9,19] making it difficult to evaluate response to therapy via routine CE-MRI. We argued that noninvasive in vivo measurement of tumor metabolic characteristics is a better method to detect diffuse infiltrative glioma, as tumor metabolism does not depend on the status of the blood–brain barrier.

Here, we investigated whether metabolic mapping via multivoxel in vivo ^{1}H MR spectroscopic imaging (MRSI) is more appropriate to detect glioma progression under anti-angiogenic therapies and we examined the effects of these therapies on tumor metabolism.

Materials and Methods

Animals

Athymic female Bagg albino (BALB)/c nu/nu mice (18–25 g, age 6–8 wk) were kept under specified pathogen free conditions and received food and water ad libitum. The local Animal Experimental Committee of the Radboud University Nijmegen Medical Centre (RUNMC) approved all experiments. E98 or E473 glioblastoma cells were injected orthotopically as described previously (~300 000 tumor cells per mouse).[15] Animals were closely monitored and subjected to MRS and MRI followed by sacrifice when evident signs of tumor burden (eg, >15% weight loss in 2 d, severe neurological abnormalities) were observed. In some cases, tumor-bearing animals were subjected to longitudinal measurements (T_2-weighted imaging and MRSI). Brains were harvested and formalin fixed and paraffin embedded for further analysis.

Therapy

Animals carrying E98 tumors were randomly divided into 3 groups. Treatment was started when signs of tumor growth became apparent, evidenced by the presence of edema in T_2-weighted MRI (characteristically at day 13 post-implantation, not shown). Bevacizumab (Avastin, Genentech) was administered twice a week at a dose of 5 mg/kg in 100 μL phosphate buffered saline (PBS) via i.p. injection ($n = 13$). XL184 (cabozantinib, a combined VEGF receptor 2/c-Met tyrosine kinase inhibitor; Exelixis) was given by oral gavage by daily dosing at 100 mg/kg ($n = 11$). Placebo-treated mice (oral administration of PBS) were used as the control group ($n = 15$). Previous studies already showed that i.p. injection of PBS did not affect tumor growth, allowing us to use this control group for both treatment regimens. Treatment of mice carrying E473 human glioma xenografts, which grow in a highly diffuse fashion, has been described before.[7] E473-carrying mice, both controls and bevacizumab treated, were also subjected to the MRSI protocol to be described here ($n = 4$ or 5).

MRI and MR Spectroscopy

Animals ($n = 4$ for each group) were anesthetized using 1%–2% isoflurane in a 70%/30% N_2O/O_2 mixture and placed in a prone position in an MR cradle. Breathing was monitored throughout the MR experiment, and the animals' core temperature was maintained at 37.5°C using a continuous flow of warm air (SA Instruments).

MR investigations were performed on a 7T animal MR system (ClinScan, Bruker BioSpin) equipped with a clinical user interface (syngo MR, Siemens). All used MR sequences were adopted from their clinical counterparts and received minor modifications to allow for optimal usage of the available gradient and radiofrequency power without compromising compatibility with the clinical (postprocessing) platform. After acquisition, data were fitted in LCModel software, and choline (Cho), N-acetyl aspartate (NAA), and lactate (having ^{1}H resonances at 3.5 and 3.19 ppm; 2.01, 2.49, and 2.67 ppm; and 1.31 ppm, respectively) in 0.85-mm^3 voxels were quantified. Cho/NAA ratios were projected as 2D heat

maps superimposed on T_2-weighted MR maps. Similarly, absolute lactate levels were depicted in heat maps. Further details on these analyses can be found in the Supplementary data. Cho/NAA ratios in sets of 4 independent voxels, chosen in CE or non-CE areas (as identified on hematoxylin and eosin [H&E] staining of corresponding sections), as well as in normal brain, were compared using a Mann–Whitney *U*-test.

CE-MRI was performed as described previously.[4] In short, after acquiring MRS data, T_1-weighted images were acquired, followed by an intravenous bolus injection of 0.2 mL of gadolinium–diethylenetriamine pentaacetic acid (Gd-DTPA; 20 mMol/L; Magnevist, Schering). Additional sets of T_1-weighted images were acquired 2 min after injection.

Immunohistochemistry

Immunohistochemical stainings were performed as described before[7] with antibodies against glucose transporter 1 (GLUT1; a constitutive marker for normal brain capillary endothelial cells and for hypoxic tumor cells; Neomarkers), monocarboxylate transformer 1 (MCT1; a lactate importer, expressed near and in glycolytic cells) and MCT4 (a lactate exporter, expressed by glycolytic cells; both MCTs from Santa Cruz Biotech), and hypoxia-inducible factor 1-alpha (HIF1α; clone 54, BD Biosciences Pharmingen). Anti–carbonic anhydrase (CA)–IX (M75) antibody was a generous gift from Dr E. Oosterwijk (RUNMC). For HIF1α staining, the signal was additionally amplified using catalyzed reporter deposition.[20] In some cases, tumor-bearing animals were injected with pimonidazole prior to sacrifice, after which the accumulated pimonidazole in hypoxic tumor areas was visualized using a specific rabbit antiserum (Hydroxyprobe Omni kit), a generous gift of Ing H. Peters (RUNMC).[21]

Results

Detectability of Glioma by MRSI

The poor visibility in CE-MRI of diffuse infiltrative areas in clinical and preclinical models of glioblastoma, a phenotype that is characteristically present in untreated tumors and is increased upon treatment with angiogenesis inhibitors,[4,9,22] led us to investigate whether the metabolic profile of tumor cells in these areas allows visualization via multivoxel MRSI. NAA is a metabolite that is synthesized by neurons in abundant amounts, whereas Cho compounds are precursors of cell membrane components that increase in cells after malignant transformation.[23] Both NAA and Cho-containing compounds (total choline, tCho) can be detected by chemical shift imaging in ^{1}H MRSI. Increased tCho and decreased NAA tissue levels are hallmarks of brain tumor growth, and tCho over NAA ratios (Cho/NAA) are increased in gliomas, discriminating tumor from normal brain tissue with a specificity of 86% and a sensitivity of 90%.[24–26] E98 xenografts present with the heterogeneous phenotypes that are also present in clinical gliomas and respond similarly to anti-angiogenic treatment with respect to loss of MRI visualization.[4,7,9] Compared with normal mouse brain (Fig. 1A), E98 xenografts present with highly elevated tCho/NAA, both in compactly growing (Fig. 1B) and diffuse infiltrative E98 areas (Fig. 1C). Panels D–F in Fig. 1 show spectra corresponding to the respective encircled voxels in panels A–C. Voxels with elevated ratios colocalize with tumor, as established by Gd-DTPA–enhanced T_1-weighted MRI (see the post/pre subtraction image in Fig. 1G) and H&E staining of corresponding brain sections (Fig. 1I and J). Note that the diffuse tumor in panel J is hardly detectable on CE-MRI (panel H) but results in elevated Cho/NAA ratios (panels C–F).

MRSI of Glioma Under Anti-angiogenic Treatment

To investigate whether the tCho/NAA ratios could be utilized for detection of diffuse infiltrative glioma under anti-angiogenic treatment, we treated E98- and E473-bearing mice with bevacizumab. Treated animals were sequentially subjected to MRSI and CE-MRI. Whereas Gd-DTPA–enhanced imaging showed a greatly diminished signal compared with that in nontreated E98 mice (Fig. 2B, compare with Fig. 1G), MRS mapping of the tCho/NAA ratio revealed extensive presence of tumor (Fig. 2A and D). Comparison with corresponding H&E-stained brain sections (Fig. 2C) showed that despite the relatively low resolution, the tumor was far better delineated by ^{1}H MRS than by CE-MRI.

To exclude that these findings were somehow specific to E98 xenografts, we performed similar experiments with the E473 xenograft model. E473 tumors grow in a diffuse infiltrative manner without evidence of an angiogenic response.[15] We previously showed that the apparent absence of angiogenesis coincides with a lack of response to bevacizumab.[7] Similar to the results obtained with E98 tumors, CE-MRI was not able to delineate tumor in E473 xenografts (Fig. 2F),[7] whereas MRSI revealed extensive tumor involvement (Fig. 2E) consistent with histology (Fig. 2G). The ratio of tCho/NAA in the CE area in Fig. 2B was 2.9 ± 0.84 (mean $\pm$ SD of 4 voxels in the red boxed area in inset) and did not differ from tCho/NAA ratios outside the CE area (2.64 ± 0.83; mean $\pm$ SD of 4 voxels in green boxed area; $P = .69$). These numbers were significantly higher than tCho/NAA ratios in voxels outside the tumor area and in nonneoplastic mouse brain (0.45 ± 0.38 and 0.49 ± 0.12, respectively; $P = .03$ for both comparisons; see Fig. 2H).

In our experience, tyrosine kinase inhibitors of VEGF receptor 2 can be more effective in normalizing tumor blood vessels in glioma xenografts than can bevacizumab.[4,7] We have previously published that cabozantinib, a tyrosine kinase inhibitor with specificity for VEGF receptor 2, Met, and Ret, fully reduces blood vessel leakage in E98 xenografts, resulting in tumors that are invisible in CE-MRI (Fig. 2J).[27] In agreement with the E98 and E473 data, MRSI heat maps of tCho/NAA were indicative of extensive tumor presence (Fig. 2I, compare with H&E staining in Fig. 2K).

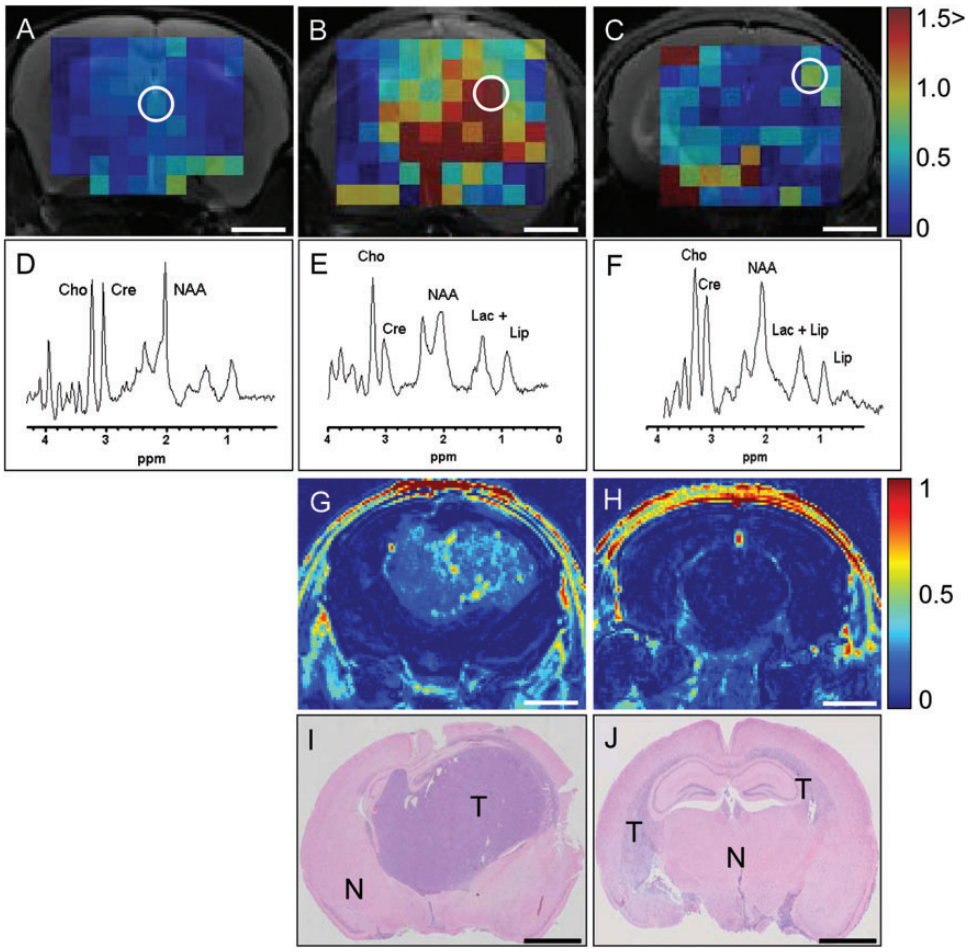

Fig. 1. MRSI visualizes the diffuse infiltrative E98 tumor component better than CE-MRI. Representative in vivo tCho/NAA (scaled 0–1.5) MRSI metabolic maps of (A) 1 non-tumor-bearing control brain and (B and C) 2 untreated brains infiltrated with E98 xenografts. E98 tumors characteristically display compact, angiogenic growth as well as diffuse infiltrative growth, the ratio of these being variable. For clarity, a tumor with profound compact growth and relatively small areas of infiltrative growth (B, E, G, I) and one with the converse ratio (C, F, H, J) are shown. Panels D–F show spectra ($T_E = 24$ ms) of the respective white encircled voxels in panels A–C. Cho, creatine (Cre), NAA, lipid, and lactate peaks are indicated. Panels G and H show contrast enhanced (Gd-DTPA) MRI delta map $(S_{post}\text{-}S_{pre})/S_{pre}$ of corresponding slices of the tumor-bearing animals. Note that contrast agent entered the brain in panels G and H, indicated by the high signal intensity in the skull and skin. Panels I and J show matched endpoint H&E histology. Size bars correspond to 2 mm. Abbreviations: T, tumor; N, normal.

Glycolysis in E98 Xenografts Is Limited to Focal Areas of Hypoxia

Inhibition of angiogenesis has been shown to result in hypoxia and an increase of glycolysis in glioma.[28] Based on the observed lack of hypoxia in diffuse areas of glioma, also after anti-angiogenic treatment,[7,29] we evaluated the extent of glycolysis during development of E98 xenografts by directly measuring tissue lactate levels in treated and nontreated E98 xenografts. In addition to MRSI at short echo time (T_E; 24 ms), we acquired data at $T_E = 144$ ms, allowing quantification of tissue lactate concentrations (representative examples shown in Fig. 3N). At this long echo time, the lactate peak at 1.3 ppm shows a characteristic inversion due to the strong J-coupling of the lactate CH_3 and CH proton spins. Furthermore, at long echo times, the contribution of overlapping lipids (as is present at $T_E = 24$ ms) is minimized by their short T_2 relaxation time.

Lactate levels were low in control-treated E98-bearing mice (Fig. 3B and E, compare with panels A, C, D, and F, which show elevated Cho/NAA levels in tumor-containing voxels; note that this is the same mouse presented in Fig. 1). Bevacizumab treatment clearly induced glycolysis, as reflected by gradually increasing lactate levels at D13, D20, and D26, representing days 0, 7, and 13 after start of treatment (Fig. 3H, J, L, mean concentration at D26: 9.9 ± 2.2 mM in compact tumor areas, as established by corresponding histology [$n = 76$ voxels] vs 2.6 mM in control mice [$n = 495$ voxels], $P < .0001$). In the tumor periphery, however, large areas of highly elevated Cho/NAA ratios were detected (Fig. 3I and K), with relatively low lactate (Fig. 3J and L). Tumor heterogeneity with respect to lactate production

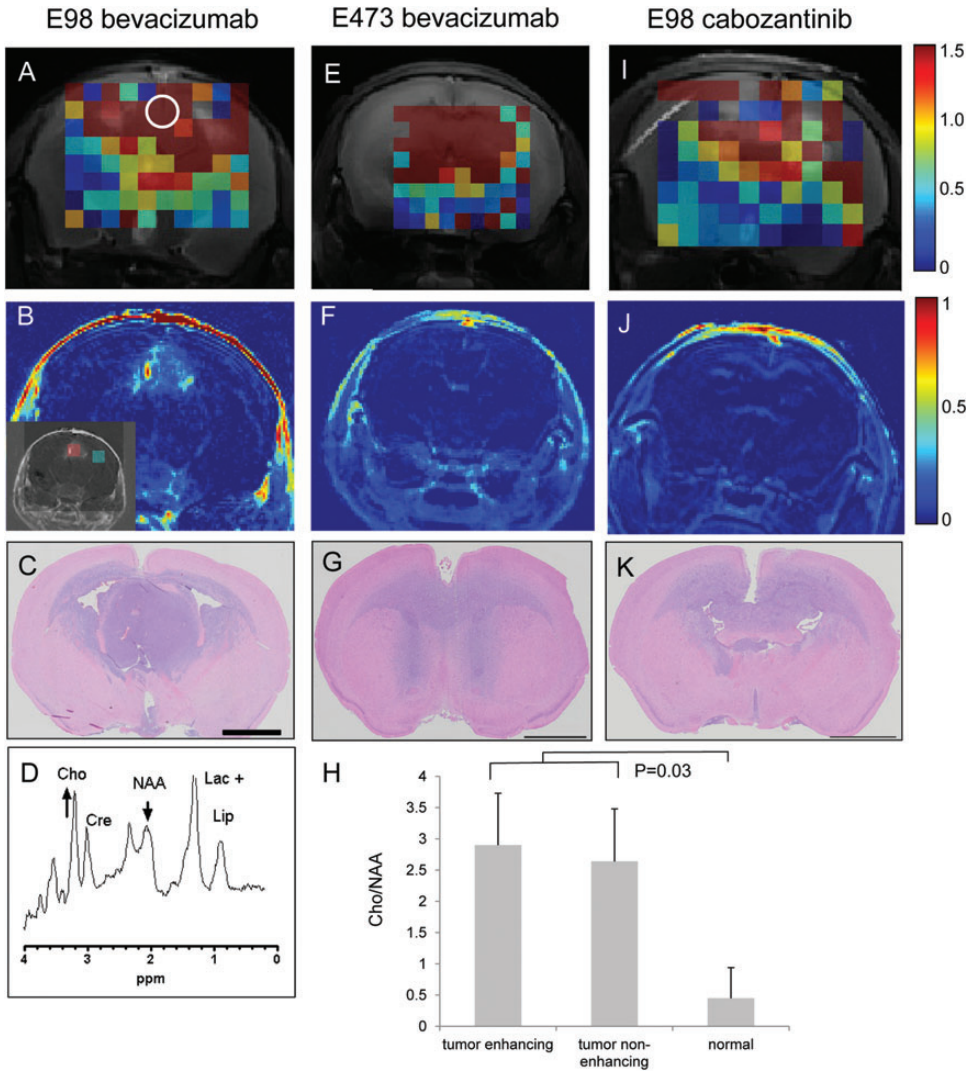

Fig. 2. MRSI visualization of bevacizumab-treated E98 xenografts. Cho/NAA (scaled 0–1.5) MRSI metabolic map of representative mouse brains with (A and I) E98 tumor or (E) E473 tumor after treatment with (A, E) bevacizumab and (I) cabozantinib. The short echo time (24 ms) spectrum of the white encircled voxel in panel A is depicted in D. Note that the MRSI correlates better with histology (H&E staining in C, G, K) than contrast enhanced (Gd-DTPA) MRI; see delta map (S_{post}-S_{pre})/S_{pre} in B, F, and J. The inset in panel B shows a red and a green area (corresponding to enhancing and non-enhancing tumor) in which Cho/NAA ratios were quantified. These data, together with Cho/NAA ratios from nonneoplastic brain, are presented in H. Size bars in C–K correspond to 2 mm. Note that only the central part of the brain is included in the metabolic maps, as the boundaries between brain and other tissues severely compromise the quality of spectra collected from these regions.

stresses the importance of performing multivoxel instead of single voxel MRSI. Importantly, after cabozantinib treatment, a number of mice showed only diffuse infiltrative growth with no detectable hypoxia markers.[27] Whereas tumor was readily detected by tCho/NAA mapping (Fig. 3N), lactate levels were even lower than after bevacizumab treatment in these mice (Fig. 3O, compare with 3P).

The diffuse infiltrative tumor that remains after antiangiogenic therapy takes advantage of the high cerebral vascular density for its blood supply. As these areas are well perfused (as indicated by the absence of hypoxia), lactate may be rapidly drained from the tumor, resulting in underestimation of lactate levels. In this scenario, glycolytic cells should express MCTs to facilitate efficient lactate secretion, and CA-IX to prevent intracellular acidosis.[30] GLUT1 and MCT4 were absent in diffusely growing tumor cells (Fig. 4A, arrows point to diffuse infiltrative cells), and this was also true for MCT1, HIF1α, and CA-IX (data not shown). Similar results were previously obtained with diffuse E473 xenografts.[7] This contrasted with the situation in compact tumor regions where significant areas stained positive for GLUT1 and MCT4 proteins in a pattern that was reminiscent of central hypoxia (arrowheads in Fig. 4A). Hypoxia was far more pronounced in compact areas in response to

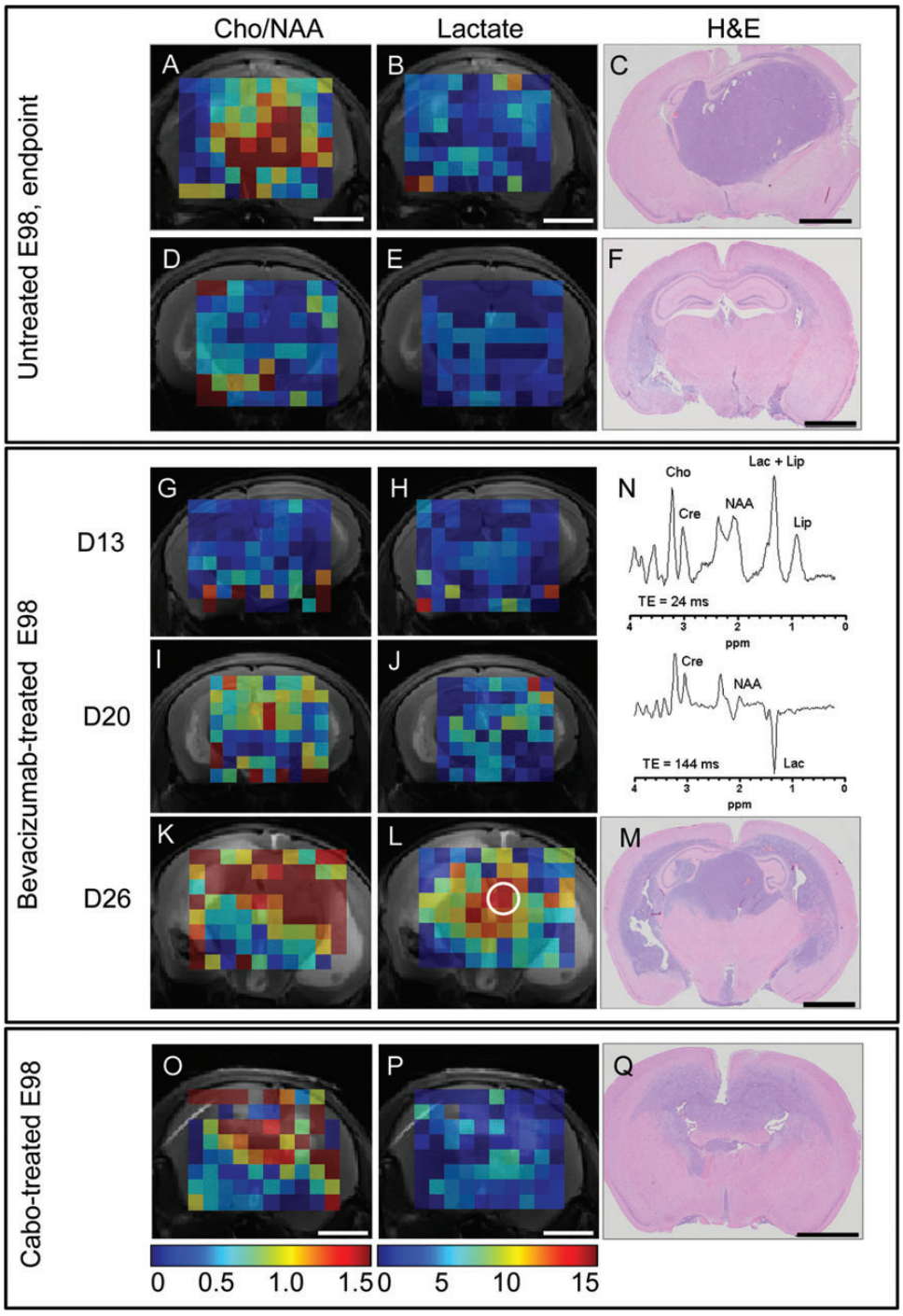

Fig. 3. Bevacizumab treatment results in a highly localized increase in lactate production in E98 xenografts. Panels A and D show maps of Cho/NAA metabolite ratios (range 0–1.5, values obtained using $T_E = 24$ ms); in panels B and E, absolute lactate concentrations are depicted (range 0–15 mM, values obtained using $T_E = 144$ ms). C and F represent H&E stained corresponding coronal sections (same animals as shown in Fig. 1). (A–F) untreated; (G–M) bevacizumab-treated. Panels G–H, I–J, and K–L represent MRS maps at days 13, 20, and 26 post tumor implantation, which corresponds to days 0, 7, and 13 of bevacizumab treatment. Note in panels J and L that lactate levels gradually increase after treatment with bevacizumab, but predominantly in compact tumor areas. Panel N shows a representative short (24 ms) and long (144 ms) echo time MR spectrum of a selected voxel of the bevacizumab-treated animal (day 26, white encircled voxel in panel L). Panels O–Q represent mouse brains with E98 xenografts after treatment with cabozantinib. Note that only low levels of lactate are observed (P), whereas high Cho/NAA ratios are detected throughout the tumor (O). All metabolite values were obtained using LCModel and plotted regardless of the Cramér–Rao lower bound value of the fits. Voxels in which one of the metabolites could not be fitted by LCModel are omitted. Size bars correspond to 2 mm.

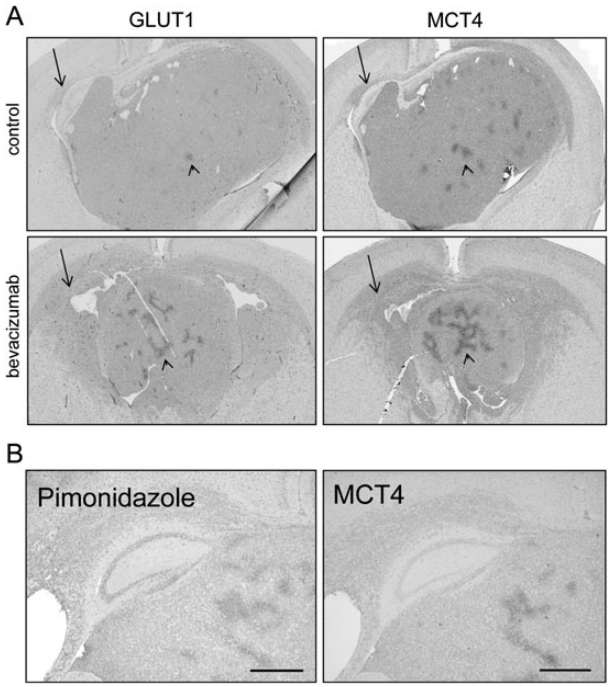

Fig. 4. Hypoxia levels in E98 xenografts upon treatment. Representative immunohistochemistry of the hypoxia markers GLUT1 and MCT4 in (A) untreated and bevacizumab-treated tumor-bearing animals. (B) MCT4 expression correlates well with pimonidazole accumulation and further demonstrates that hypoxia is limited to foci in central compact tumor areas only. Size bars: 1 mm.

bevacizumab treatment (lower panels in Fig. 4A), and this is in agreement with previous data.[7]

To further prove that excessive glycolysis in our models was confined to areas of hypoxia, we injected mice just before sacrifice with pimonidazole, accumulation of which is the gold standard for hypoxia,[31] and stained serial sections of treated E98 xenografts for GLUT1, MCT4, and pimonidazole. As shown in Fig. 4B, MCT4 especially had a strong colocalization with pimonidazole, and this staining pattern largely colocalized with GLUT1 (data not shown).

In conclusion, comparison of the lactate map in Fig. 3L with histological analysis in Fig. 3M and immunohistochemical data from Fig. 4 strongly suggests that elevated lactate levels concentrate in areas of hypoxia. The absence of glycolysis-related proteins in diffuse tumor areas, together with the absence of elevated lactate levels, suggests that tumor cells in these areas do not excessively depend on glycolysis for their growth.

Discussion

The lack of reliable modalities to visualize the diffuse infiltrative component of glioblastoma, especially after treatment with anti-angiogenic compounds, is a serious problem in neuro-oncology. The necessity for novel imaging modalities is emphasized by the recent finding from randomized clinical trials that despite dramatic radiological responses upon bevacizumab treatment, overall survival of glioblastoma patients was not improved.[32,33]

CE-MRI is the common standard in routine examinations of brain tumors, but it is not able to delineate the entire tumor volume, and detectability is even more decreased upon VEGF inhibition, a phenomenon that was confirmed in multiple orthotopic glioma xenograft models after treatment with different anti-angiogenic compounds.[4,7] Recently, new guidelines for response assessment of high-grade gliomas were proposed by the Revised Assessment in Neuro-Oncology consortium, in which T_2-weighted and fluid-attenuated inversion recovery (FLAIR) imaging is used to detect invasive nonenhancing tumor areas.[34] T_2-FLAIR imaging visualizes tumors to some extent but has a number of limitations as well. Again, therapy may complicate T_2-based tumor detection[18] due to vessel normalization and resulting edema reduction. We routinely performed T_2-weighted imaging of the mice in the current study and indeed found that T_2-weighted imaging in general was a less reliable measure of tumor volume (not shown).

Thus, novel diagnostic modalities that properly visualize tumor extent and provide patients with realistic information on therapeutic effects and prognosis are urgently needed. In recent years, specific physiological and metabolic MR methods have been implemented to assess response to brain tumor treatment, such as imaging relative cerebral blood volume, water diffusion in tissue (diffusion weighted imaging), and MRSI of metabolites.[26,35–39] The potential of these approaches to reliably detect tumor load and spread and thus to circumvent the registration of mainly pseudoresponses in anti-angiogenic treatments is currently a topic of intense research. As proper validation of this potential may be difficult in patients, studies of orthotopically growing human brain tumors in animals is important for validation.

We show here in 2 independent orthotopic glioma xenograft models, both displaying the characteristic diffuse infiltrative growth of glioma, that ^{1}H MRSI of tCho/NAA ratios identifies the presence of infiltrative tumor tissue better than CE-MRI. This metabolism-based visualization is not hampered by vessel-normalizing effects (ie, functional restoration of blood–brain barrier) of anti-angiogenic compounds. With increasing accessibility of high-field MR equipment and robust spectroscopic imaging acquisition software also in the clinic,[40,41] inclusion of ^{1}H MRSI–based visualization of glioblastoma growth becomes feasible and an attractive and promising modality. Of importance, this technology may also yield further information on the metabolic status of tumors that could aid in tumor classification.[42]

Whereas bevacizumab treatment resulted in increased hypoxia in E98 xenografts, corroborating a previous report,[28] our multivoxel analysis revealed that lactate levels were increased in areas of hypoxia only. Cabozantinib treatment resulted in predominantly diffuse infiltrative tumors, often without any sign of hypoxia, and this was corroborated by the absence of

significantly elevated levels of lactate. The combined findings suggest that anti-angiogenic treatment induces glycolysis only in compactly growing areas in which a rapid shutdown of blood supply may result in local hypoxic conditions. Possibly, the local shutdown of blood supply and the resulting poor washout in glycolytic areas contributes to even higher accumulation of lactate. Also in E473 glioma xenografts, no glycolysis markers could be detected, even after treatment with bevacizumab.[7] Our finding of limited glycolysis in glioma is therefore not a one-model artifact. Furthermore, since glycolysis markers cannot be found in diffuse infiltrating tumor cells in clinical samples,[43] these findings seem to have clinical relevance. Recent studies in glioma patients and in mice carrying orthotopic patient-derived glioma xenografts revealed that in glioma, mitochondrial oxidative phosphorylation predominates over glycolysis.[44,45] This is in line with our findings and does not conform to the Warburg hypothesis that tumor cells depend more on glycolysis than on mitochondrial oxidative phosphorylation.[46] It is likely that the potential for extensive vessel co-option by glioma cells, a result of the dense vascular bed in the brain, equips the diffusely infiltrating glioma cells with sufficient oxygen and nutrients to allow mitochondrial metabolism to proceed. Only in highly proliferative tumor areas that outgrow the local blood supply may hypoxia develop, resulting in a shift of the glycolysis/oxidative phosphorylation equilibrium toward glycolysis. In a previous report, a symbiotic relationship was suggested between hypoxic and normoxic tumor areas.[47] In this paper it is suggested that lactate, produced by hypoxic cells, is taken up by normoxic cells via MCT1. As we did not find increased MCT1 expression in diffuse infiltrative tumor cells in our models, it is not clear to what extent this phenomenon applies to our xenografts.

Glycolysis is gaining interest as a therapeutic target—for instance, with inhibitors like dichloroacetate.[48] This pyruvate dehydrogenase kinase inhibitor has been proposed as a potential adjuvant treatment to bevacizumab.[28] Indeed, cells that shifted their metabolism to glycolysis as a result of bevacizumab treatment would be forced to turn to mitochondrial oxidative phosphorylation and this would result in cell death in the absence of oxygen.[49–53] Our data show that the effects of glycolysis inhibition on E98 tumor growth would be limited to hypoxic tumor areas, leaving the larger volume of diffuse infiltrative tumor unaffected.

Yet, the highly heterogeneous nature of clinical glioblastoma makes it worthwhile to generate ^{1}H MRS–based maps of Cho/NAA and lactate. Patients in whom a significant fraction of the tumor is glycolytic (as determined by the total voxel volume with elevated lactate/total voxel volume with elevated Cho/NAA) may indeed significantly benefit from therapy with dichloroacetic acid. In this way MRSI can help in selecting patients who are eligible for antiglycolytic treatment.

Besides pruning of newly formed vessels, bevacizumab treatment has been proposed to normalize tumor blood vessels and improve tumor perfusion and oxygenation, thereby increasing susceptibility to radio- and chemotherapy.[54] In our study, treatment with bevacizumab increased the hypoxic tumor cell fraction in compact E98 areas, an effect that was also seen previously with vandetanib.[9] This is in agreement with a model in which bevacizumab rapidly decreases blood flow to compact growing tumor areas, rather than improving perfusion. We propose that anti-angiogenic treatment of tumor areas that have undergone the angiogenic switch[55] will result in consolidation of vasculature in these areas. Continuing tumor expansion in the absence of novel vascularization (initially via vascular co-option[3]) will result in increased hypoxia. On the other hand, in earlier-stage tumors in which the angiogenic switch did not yet occur, treatment would prevent development of these areas, resulting in diffuse tumor growth exclusively.

In conclusion, we have shown that MRSI is superior to CE-MRI for a reliable noninvasive evaluation of therapeutic effects in the anti-angiogenic treatment of gliomas and yields additional information about tumor metabolism that may be exploited for individualized treatment. We further showed that infiltrating glioma cells in our models did not display the glycolytic phenotype that has been suggested to be a hallmark of tumors (ie, the Warburg effect).

Supplementary Material

Supplementary material is available online at *Neuro-Oncology* (http://neuro-oncology.oxfordjournals.org/).

Funding

This work was supported by the Dutch Organisation for Scientific Research (NWO-middelgroot 40–00506–90-0602, NWO BIG [VISTA]), the Dutch Brain Foundation (grant KS2010(1)-01 to W. L.), and the Radboud University Centre for Oncology (RUCO to A. C. N.).

Acknowledgments

We thank Dr Wiljan Hendriks for helpful discussions, Andor Veltien for technical assistance with MR measurements, and Sjaak van Asten for help with MRSI postprocessing. We are grateful to Jeroen van der Laak for his help with statistical analyses and to Dr Egbert Oosterwijk, Prof Floris Rutjes, and Ing Hans Peters for providing M75 antibody, pimonidazole, and pimonidazole antiserum, respectively. We are grateful to Geert Poelen, Aglaja Zwiers, Jeroen Mooren, and Bianca Lemmers van de Weem for assistance with performing the animal experiments.

Conflict of interest statement. None declared.

References

1. Stupp R, Hegi ME, Mason WP, et al. Effects of radiotherapy with concomitant and adjuvant temozolomide versus radiotherapy alone on survival in glioblastoma in a randomised phase III study: 5-year analysis of the EORTC-NCIC trial. *Lancet Oncol*. 2009;10(5):459–466.
2. Wesseling P, Ruiter DJ, Burger PC. Angiogenesis in brain tumors: pathobiological and clinical aspects. *J Neurooncol*. 1997;32(3):253–265.
3. Leenders W, Kusters B, De Waal R. Vessel co-option: how tumors obtain blood supply in the absence of sprouting angiogenesis. *Endothelium*. 2002;9:83–87.
4. Claes A, Gambarota G, Hamans B, et al. Magnetic resonance imaging–based detection of glial brain tumors in mice after antiangiogenic treatment. *Int J Cancer*. 2008;122(9):1981–1986.
5. Verhoeff JJ, van Tellingen O, Claes A, et al. Concerns about antiangiogenic treatment in patients with glioblastoma multiforme. *BMC Cancer*. 2009;9(1):444.
6. de Groot JF, Fuller G, Kumar AJ, et al. Tumor invasion after treatment of glioblastoma with bevacizumab: radiographic and pathologic correlation in humans and mice. *Neuro Oncol*. 2010;12(3):233–242.
7. Navis AC, Hamans BC, Claes A, et al. Effects of targeting the VEGF and PDGF pathways in diffuse orthotopic glioma models. *J Pathol*. 2011; 223(5):626–634.
8. Narayana A, Kelly P, Golfinos J, et al. Antiangiogenic therapy using bevacizumab in recurrent high-grade glioma: impact on local control and patient survival. *J Neurosurg*. 2009;110(1):173–180.
9. Claes A, Wesseling P, Jeuken J, Maass C, Heerschap A, Leenders WP. Antiangiogenic compounds interfere with chemotherapy of brain tumors due to vessel normalization. *Mol Cancer Ther*. 2008;7(1):71–78.
10. Jain RK, di Tomaso E, Duda DG, Loeffler JS, Sorensen AG, Batchelor TT. Angiogenesis in brain tumours. *Nat Rev Neurosci*. 2007;8(8):610–622.
11. Norden AD, Drappatz J, Wen PY. Antiangiogenic therapy in malignant gliomas. *Curr Opin Oncol*. 2008;20(6):652–661.
12. Plate KH, Scholz A, Dumont DJ. Tumor angiogenesis and anti-angiogenic therapy in malignant gliomas revisited. *Acta Neuropathol*. 2012;124(6): 763–775.
13. Vredenburgh JJ, Desjardins A, Herndon JE 2nd, et al.Bevacizumab plus irinotecan in recurrent glioblastoma multiforme. *J Clin Oncol*. 2007;25(30): 4722–4729.
14. Friedman HS, Prados MD, Wen PY, et al. Bevacizumab alone and in combination with irinotecan in recurrent glioblastoma. *J Clin Oncol*. 2009; 27(28):4733–4740.
15. Claes A, Schuuring J, Boots-Sprenger S, et al. Phenotypic and genotypic characterization of orthotopic human glioma models and its relevance for the study of anti-glioma therapy. *Brain Pathol*. 2008;18(3):423–433.
16. Gambarota G, Leenders W, Maass C, et al. Characterisation of tumour vasculature in mouse brain by USPIO contrast-enhanced MRI. *Br J Cancer*. 2008;98(11):1784–1789.
17. Lamszus K, Kunkel P, Westphal M. Invasion as limitation to anti-angiogenic glioma therapy. *Acta Neurochir Suppl*. 2003;88:169–177.
18. Batchelor TT, Sorensen AG, di Tomaso E, et al. AZD2171, a pan-VEGF receptor tyrosine kinase inhibitor, normalizes tumor vasculature and alleviates edema in glioblastoma patients. *Cancer Cell*. 2007;11: 83–95.
19. Kamoun WS, Ley CD, Farrar CT, et al. Edema control by cediranib, a vascular endothelial growth factor receptor–targeted kinase inhibitor, prolongs survival despite persistent brain tumor growth in mice. *J Clin Oncol*. 2009;30:30.
20. Bobrow MN, Harris TD, Shaughnessy KJ, Litt GJ. Catalyzed reporter deposition, a novel method of signal amplification. Application to immunoassays. *J Immunol Methods*. 1989;125(1–2):279–285.
21. van Laarhoven HW, Bussink J, Lok J, Punt CJ, Heerschap A, van Der Kogel AJ. Effects of nicotinamide and carbogen in different murine colon carcinomas: immunohistochemical analysis of vascular architecture and microenvironmental parameters. *Int J Radiat Oncol Biol Phys*. 2004;60(1): 310–321.
22. Claes A, Leenders W. Vessel normalization by VEGF inhibition. *Cancer Biol Ther*. 2008;7(7):7.
23. Glunde K, Bhujwalla ZM, Ronen SM. Choline metabolism in malignant transformation. *Nat Rev Cancer*. 2011;11(12):835–848.
24. McKnight TR, von dem Bussche MH, Vigneron DB, et al. Histopathological validation of a three-dimensional magnetic resonance spectroscopy index as a predictor of tumor presence. *J Neurosurg*. 2002;97(4):794–802.
25. Li X, Jin H, Lu Y, Oh J, Chang S, Nelson SJ. Identification of MRI and 1H MRSI parameters that may predict survival for patients with malignant gliomas. *NMR Biomed*. 2004;17(1):10–20.
26. Nelson SJ. Assessment of therapeutic response and treatment planning for brain tumors using metabolic and physiological MRI. *NMR Biomed*. 2011;24(6):734–749.
27. Navis AC, Bourgonje A, Wesseling P, et al. Effects of dual targeting of tumor cells and stroma in human glioblastoma xenografts with a tyrosine kinase inhibitor against c-MET and VEGFR2. *PLoS One*. 2013;8(3): e58262.
28. Keunen O, Johansson M, Oudin A, et al. Anti-VEGF treatment reduces blood supply and increases tumor cell invasion in glioblastoma. *Proc Natl Acad Sci U S A*. 2011;108(9):3749–3754.
29. Roodink I, van der Laak J, Kusters B, et al. Development of the tumor vascular bed in response to hypoxia-induced VEGF-A differs from that in tumors with constitutive VEGF-A expression. *Int J Cancer*. 2006;119(9): 2054–2062.
30. Swietach P, Hulikova A, Vaughan-Jones RD, Harris AL. New insights into the physiological role of carbonic anhydrase IX in tumour pH regulation. *Oncogene*. 2010;29(50):6509–6521.
31. Raleigh JA, Chou SC, Arteel GE, Horsman MR. Comparisons among pimonidazole binding, oxygen electrode measurements, and radiation response in C3H mouse tumors. *Radiat Res*. 1999;151(5):580–589.
32. Gilbert M. RTOG 0825: phase III double-blind, placebo-controlled trial evaluating bevacizumab in patients with newly diagnosed glioblastoma. ASCO Annual Proceedings 2013;31, suppl abstract 1.
33. Tabatabai G, Felsberg J, Sabel M, et al. Bevacizumab failure in glioblastomas. ASCO Annual Proceedings 2012;30, suppl abstract 2067.
34. Wen PY, Macdonald DR, Reardon DA, et al. Updated response assessment criteria for high-grade gliomas: Response Assessment in Neuro-Oncology working group. *J Clin Oncol*. 2010;28(11):1963–1972.
35. Pechman KR, Donohoe DL, Bedekar DP, Kurpad SN, Hoffmann RG, Schmainda KM. Characterization of bevacizumab dose response relationship in U87 brain tumors using magnetic resonance imaging measures of enhancing tumor volume and relative cerebral blood volume. *J Neurooncol*. 2011;105(2):233–239.
36. Ellingson BM, Malkin MG, Rand SD, et al. Volumetric analysis of functional diffusion maps is a predictive imaging biomarker for cytotoxic and anti-angiogenic treatments in malignant gliomas. *J Neurooncol*. 2011;102(1): 95–103.

37. LaViolette PS, Cohen AD, Prah MA, et al. Vascular change measured with independent component analysis of dynamic susceptibility contrast MRI predicts bevacizumab response in high-grade glioma. *Neuro Oncol*. 2013;15(4):442–450.
38. Hygino da Cruz LC, Jr., Rodriguez I, Domingues RC, Gasparetto EL, Sorensen AG. Pseudoprogression and pseudoresponse: imaging challenges in the assessment of posttreatment glioma. *AJNR Am J Neuroradiol*. 2011;32(11):1978–1985.
39. Hoff BA, Bhojani MS, Rudge J, et al. DCE and DW-MRI monitoring of vascular disruption following VEGF-Trap treatment of a rat glioma model. *NMR Biomed*. 2012;25(7):935–942.
40. Scheenen TW, Klomp DW, Wijnen JP, Heerschap A. Short echo time 1H-MRSI of the human brain at 3 T with minimal chemical shift displacement errors using adiabatic refocusing pulses. *Magn Reson Med*. 2008;59(1):1–6.
41. Horska A, Barker PB. Imaging of brain tumors: MR spectroscopy and metabolic imaging. *Neuroimaging Clin N Am*. 2010;20(3):293–310.
42. Tate AR, Underwood J, Acosta DM, et al. Development of a decision support system for diagnosis and grading of brain tumours using in vivo magnetic resonance single voxel spectra. *NMR Biomed*. 2006;19(4):411–434.
43. Roodink I, Raats J, van der Zwaag B, et al. Plexin D1 expression is induced on tumor vasculature and tumor cells: a novel target for diagnosis and therapy? *Cancer Res*. 2005;65(18):8317–8323.
44. Marin-Valencia I, Yang C, Mashimo T, et al. Analysis of tumor metabolism reveals mitochondrial glucose oxidation in genetically diverse human glioblastomas in the mouse brain in vivo. *Cell Metab*. 2012;15(6):827–837.
45. Maher EA, Marin-Valencia I, Bachoo RM, et al. Metabolism of [U-13 C]glucose in human brain tumors in vivo. *NMR Biomed*. 2012;25(11):1234–1244.
46. Zheng J. Energy metabolism of cancer: Glycolysis versus oxidative phosphorylation (review). *Oncol Lett*. 2012;4(6):1151–1157.
47. Sonveaux P, Vegran F, Schroeder T, et al. Targeting lactate-fueled respiration selectively kills hypoxic tumor cells in mice. *J Clin Invest*. 2008;118(12):3930–3942.
48. Wolf A, Agnihotri S, Guha A. Targeting metabolic remodeling in glioblastoma multiforme. *Oncotarget*. 2010;1(7):552–562.
49. Chen Y, Cairns R, Papandreou I, Koong A, Denko NC. Oxygen consumption can regulate the growth of tumors, a new perspective on the Warburg effect. *PLoS One*. 2009;4(9):e7033.
50. Papandreou I, Goliasova T, Denko NC. Anticancer drugs that target metabolism: is dichloroacetate the new paradigm? *Int J Cancer*. 2011;128(5):1001–1008.
51. Michelakis ED, Sutendra G, Dromparis P, et al. Metabolic modulation of glioblastoma with dichloroacetate. *Sci Transl Med*. 2010;2(31):31ra34.
52. Goldberg MS, Sharp PA. Pyruvate kinase M2-specific siRNA induces apoptosis and tumor regression. *J Exp Med*. 2012;209(2):217–224.
53. Hamanaka RB, Chandel NS. Targeting glucose metabolism for cancer therapy. *J Exp Med*. 2012;209(2):211–215.
54. Jain RK. Normalization of tumor vasculature: an emerging concept in antiangiogenic therapy. *Science*. 2005;307(5706):58–62.
55. Hanahan D, Folkman J. Patterns and emerging mechanisms of the angiogenic switch during tumorigenesis. *Cell*. 1996;86(3):353–364.